JCIM JOURNAL OF CHEMICAL INFORMATION AND MODELING

Article

Cite This: J. Chem. Inf. Model. 2019, 59, 5126−5134

pubs.acs.org/jcim

Molecular Docking as a Promising Predictive Model for Silver Nanoparticle-Mediated Inhibition of Cytochrome P450 Enzymes

Nootcharin Wasukan,[†] Mayuso Kuno,[‡] and Rawiwan Maniratanachote*[,†]

[†]National Science and Technology Development Agency (NSTDA), 111 Thailand Science Park, Khlong Luang, Pathum Thani 12120, Thailand

[‡]Department of Chemistry, Faculty of Science, Srinakharinwirot University, Sukhumwit 23, Wattana District, Bangkok 10110, Thailand

Supporting Information

ABSTRACT: Cytochrome P450 (CYP) enzymes are responsible for oxidative metabolisms of a large number of xenobiotics. In this study, we investigated interactions of silver nanoparticles (AgNPs) and silver ions (Ag^+) with six CYP isoforms, namely, CYP1A2, CYP2C9, CYP2C19, CYP2D6, CYP2E1, and CYP3A4, within CYP-specific inhibitor-binding pockets by molecular docking and quantum mechanical (QM) calculations. The docking results revealed that the Ag_3 cluster, not Ag^+, interacted with key amino acids of CYP2C9, CYP2C19, and CYP2D6 within a distance of about 3 Å. Moreover, the QM analysis confirmed that the amino acid residues of these CYP enzymes strongly interacted with the Ag_3 cluster, providing more insight into the mechanism of the potential inhibition of CYP enzyme activities. Interestingly, these results are consistent with previous in vitro data indicating that AgNPs inhibited activities of CYP2C and CYP2D in rat liver microsomes. It is suggested that the Ag_3 cluster is a minimal unit of AgNPs for in silico modeling. In summary, we demonstrated that molecular docking, together with QM analysis, is a promising tool to predict AgNP-mediated CYP inhibition. These methods are useful for deeper understanding of reaction mechanisms and could be used for other nanomaterials.

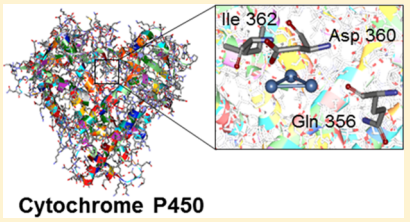

INTRODUCTION

Silver nanoparticles (AgNPs) are being incorporated into consumer products at an ever increasing pace.[1] Because of their potent antimicrobial properties and other capabilities of their modified functions, AgNPs are applied in food packaging, medical devices, personal care products, house-hold items, and nutraceutical supplements.[2−6] Production and application of these products may lead to exposure of the NPs via inhalation, ingestion, and dermal contact. Because of their very small size, once the NPs are absorbed, they can disperse throughout the body via blood circulation. A major target organ for AgNPs is the liver, which is the principal organ of drug metabolism.[7−10] Cytochrome P450 (CYP) is a superfamily of phase I drug-metabolizing enzymes, characterized by the heme prosthetic group (Figure 1a). Hepatic CYP isoforms in CYP1, CYP2, and CYP3 families are responsible for oxidative metabolisms of a large number of drugs, chemicals, and endogenous substances. Some of these substrates can also be inhibitors as well as inducers of individual CYP enzyme in human. Inhibition of CYP enzymes is of particular clinical significance because coadministration of drugs that are metabolized by the same CYP enzymes can decrease drug efficacy leading to therapeutic failure, or worse, increase drug side effects and toxicity.[11−13] The information on toxicokinetics of nanomaterials is still quite limited because of a large number of different types of nanomaterials and time required to investigate these properties in animals. While investigations performed in vivo are critical for definitively assigning toxicological properties for clinical use,[14] "3R principle" (i.e., reduce, refine, and replace the use of animals) is increasingly being promoted for routine nonclinical safety testing at the international level.[15] For this reason, we proposed to use in silico computational simulation as a powerful tool for in-depth evaluation of chemical−biomolecule interactions, and these models can be collaborated with in vitro data for prediction of chemical safety.

Molecular docking studies play an important role in computer-based predictions and estimation of three-dimensional structures of protein−ligand complexes and their interactions. The methodology can also be applied to metal NPs and protein targets such as cadmium oxide NPs for inhibition of cancerous proteins[16] and palladium NP interaction with viral protein templates (VP6).[17] In addition, quantum mechanics (QM) calculation can provide detailed insight into intrinsic reactivity of the complexes. Therefore, molecular docking and QM calculation are powerful tools in drug design and development, such as prediction of molecular structures, drug interactions and enzyme reactions. For instant, the study on CYP enzymes involved in metabolisms of cyclohexene, propene, and benzene.[18−20] The oxidation of various compounds by human CYP enzymes such as aromatic hydroxylation of tyramine via human CYP2D6 and oxidation of diclofenac, *S*-ibuprofen and *S*-warfarin by CYP2C9 were uncovered by using QM calculations.[21,22] Therefore, we sought

Received: July 12, 2019
Published: November 12, 2019

DOI: 10.1021/acs.jcim.9b00572
J. Chem. Inf. Model. 2019, 59, 5126−5134

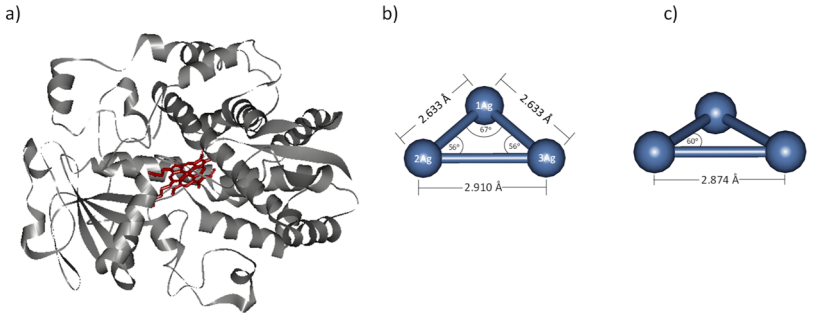

Figure 1. (a) Representative structures of a three-dimensional fold of CYP containing heme (red color); (b) the optimized Ag_3 clusters in the C_{2v} symmetry and (c) D_{3h} symmetry.

to gain insights into the interaction of AgNPs and their dissociated form of silver ion (Ag^+), with crucial hepatic CYP isoforms including CYP1A2, CYP2C9, CYP2C19, CYP2D6, CYP2E1, and CYP3A4, using molecular docking predictive model and QM calculations. The results were also compared with our previous in vivo study. This study is the first report on using in silico modeling to predict and explain the inhibition of CYP enzymes by AgNPs at the molecular level.

MATERIALS AND METHODS

Preparation of Protein Structures. Six protein structures closely related to the CYP were selected, including CYP1A2, CYP2C9, CYP2C19, CYP2D6, CYP2E1, and CYP3A4. X-ray crystallographic structures of proteins were downloaded from the Protein Data Bank (PDB) (http://www.pdb.rcsb.org). The corresponding PDB codes for these CYP proteins were 2hi4, 1r9o, 4gqs, 4xrz, 3gph, and 5te8.[23−29]

Preparation of Ag_3 Clusters and Inhibitor Structures. In computational simulation, the structure of AgNPs was modeled as Ag_3 clusters containing three atoms of silver with two different symmetries of C_{2v} and D_{3h} point groups. The molecular structure of inhibitors of each CYP enzyme, including furafylline, sulfaphenazole, *N*-3-benzyl-phenobarbital, quinidine, 4-methylpyrazole, and ketoconazole in the ground state was optimized by the density functional theory method using B3LYP functional with the 6-31G(d,p) basis set, except for the silver atoms. All of the theoretical calculations were performed using the Gaussian 09 program package.[30] An optimized geometry of each structure was used for further computational docking analysis.

Molecular Docking. The AutoDock 4.2 docking program[31] was used to investigate the interaction between silver and CYP enzymes. As the first step, the reliability of docking process was confirmed by redocking of cocrystalized ligand in the CYP enzyme pocket. The root-mean-square deviation (rmsd) between the cocrystallized and redocked conformation was investigated. The rmsd value of <2.00 Å was considered accurate in predicting binding orientation of ligand. In the docking simulation, the grid box size was set at 40 × 40 × 40 Å with a space of 0.375 Å located at the center of the macromolecule in the crystal structure of CYP enzymes. The binding modes of the ligands and human CYP enzymes were predicted by using the Lamarckian genetic algorithm. The docking parameters were set for a population size of 150. The number of GA runs was 150, and the maximum amount of generation was set at 27 000 for each docking study. The default settings were selected for all docking parameters in each experiment. Furthermore, the docked complex structures of the ligands and the surrounding amino acid residues within the radius of about 3 Å were analyzed using a BIOVIA Discovery Studio Visualizer.[32]

Quantum Mechanics Calculations. The hybrid meta exchange correlation functional, M06, with double exchange amount of nonlocal exchange called M06-2X[33] was performed by using Gaussian 09 program package.[30] In addition, the M06-2X method provided reliable results for broad applicability to chemistry.[34] In order to investigate the interaction between the binding mode of CYP enzymes and the Ag_3 cluster, the M06-2X with 6-31G(d,p) basis set was applied, and except for the Ag atom, the 3-21G basis set was used. The starting model of CYP enzyme binding site with the Ag_3 cluster complex was obtained from the Protein Data Bank. The model system of each CYP enzyme was presented in the binding pocket obtained by at least one atom interacting with any atom of the Ag_3 cluster within 7 Å diameter. Based on this structure, the model system consists of the amino acid between 25 and 31 residues. All residues were terminated if they were not connected to another residue in the selected model by a link with an acetyl group (CH_3CO-) and a methyl group ($-NHCH_3$) at the N- and C-terminal ends of the cut residues, respectively, from the adjacent residues as presented in the backbone geometries of the X-ray structure (Figure 2).

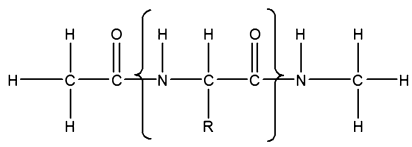

Figure 2. Capped groups of the terminal ends of chains.

Hydrogen atoms were added to the geometrical structure to generate a complete structure of the model system, and their positions were optimized based on heavy atoms being fixed. Then, the semi-empirical PM6 method was applied.[35]

This structure was used as the starting geometry to calculate the interaction energy. Moreover, zero point energy (ZPE) correction based on the vibrational motion of the molecular system was used to optimize geometries of structures. ZPE is a correction term that needs to be added to the electronic energy. It can be obtained by computing and comparing the total energy of the cluster.[36] The individual interaction energies of the Ag_3 cluster−amino acid were calculated with ZPE corrections using the following equations

$$\Delta E_0 = IE_{(Ag_3+Xi)} + IE^0_{(Ag_3+Xi)} \quad (1)$$

DOI: 10.1021/acs.jcim.9b00572
J. Chem. Inf. Model. 2019, 59, 5126−5134

$$IE_{(Ag_3+Xi)} = E_{(Ag_3+Xi)} - E_{(Ag_3)} - E_{(Xi)} \quad (2)$$

where ΔE_0 is the interaction energy included with the ZPE correction. $IE_{(Ag_3+Xi)}$ is the interaction energy of Ag_3 cluster and each amino acid residue. $E_{(Ag_3)}$ and $E_{(Xi)}$ are energies of Ag_3 cluster and each amino acid residue, respectively. IE^0 represents the ZPE correction.[37]

Natural bond orbital (NBO) analysis is an effective method for studying intra and intermolecular bonding and interaction among bonds in the molecular system.[38] In this study, NBO calculations were carried out by evaluating all possible orbital interaction energies between bonding (donor) and antibonding (acceptor) orbitals. The stabilization energy of the molecule occurs by hyperconjugative interactions, and charge delocalization has been analyzed using the second order perturbation theory. It can be calculated using the following eq 3

$$E(2) = \Delta E_{ij} = q_i \frac{F_{(i,j)}^2}{E_j - E_i} \quad (3)$$

where $E(2)$ is the stabilization energy. $\Delta E_{ji} = E_j - E_i$ is the orbital energy difference between the acceptor (j) and donor (i) NBO. q_i is the donor orbital occupancy number, and $F_{(i,j)}$ is the off diagonal elements of the fock matrix in the NBO basis.[39,40]

Furthermore, NBO analysis has been performed on the optimized structures of Ag_3 cluster−amino acid using the same level of theory and basis set, which is implemented in Gaussian 09.[30]

RESULTS AND DISCUSSION

Geometric Structures. The geometric structures of silver clusters are significant because of their functions in photography, catalysis, and designing new electronic materials.[41] Thus, a lot of information is required for computational predictions of the geometric structures of silver clusters. In recent years, various silver clusters of AgNPs such as small metal neutral Ag_n (n = 2−22), Ag_n (n = 3−9), and Ag_n (n = 5−9) have been studied.[41−46] According to the relevant literatures on Ag_n clusters, n is the number of atoms, which can be up to 160 atoms.[47−49] Geometric structures of simple species of silver clusters can provide insight into possible interactions with more complicated clusters and with specific sites on a crystal structure. In this work, we demonstrated optimized geometric structures of silver clusters up to three atoms (Ag_3). It was found that Ag_3 has two types of symmetries: C_{2v} and D_{3h}. As presented in Figure 1b, the geometry optimization of the Ag_3 (C_{2v}) consisted of three Ag atoms labeled 1Ag, 2Ag, and 3Ag, with the two-side symmetry. The calculated results showed that the theoretical bond lengths of Ag_3 (C_{2v}) were 2.910, 2.633, and 2.633 Å with the angles of 67, 56, and 56°. However, the Ag_3 (D_{3h}) showed an equal symmetry in all sides with bond lengths of 2.874 Å and angles of 60° (Figure 1c).

Docking Studies of Ag_3 Clusters with CYP Enzymes. Molecular docking approaches could provide insights into interactions between proteins and ligands. We used the optimized structures of Ag^+, Ag_3 (C_{2v}), and Ag_3 (D_{3h}) for molecular docking with CYP enzymes. Before the docking analysis, we performed redocking procedures for all six CYP enzymes and calculated rmsd for the structure conformations of the reference ligands. The obtained rmsd values were 0.698 to 1.659 Å, revealing that the X-ray crystal structures of all CYP proteins work well and could be used for further analysis. The conformations of CYP ligand complexes with the lowest binding energy were determined as the most stable binding mode. To investigate the inhibition of CYP enzymes by AgNPs, highly selective inhibitors of each CYP enzyme, including furafylline, sulfaphenazole, *N*-3-benzyl-phenobarbital, quinidine, 4-methylpyrazole, and ketoconazole, were also used in molecular docking for CYP1A2, CYP2C9, CYP2C19, CYP2D6, CYP2E1, and CYP3A4, respectively.[50−56] The amino acid residues of CYPs bound with their selective inhibitors are shown in Table 1 and Figure S1 of the Supporting Information. For ionic silver, we found that Ag^+ interacted with several amino acid residues of these CYP isoforms but not with key amino acids at active sites of CYP inhibition (Figure 3, Table 1). Meanwhile, both Ag_3 (C_{2v}) and Ag_3 (D_{3h}) clusters demonstrated interactions with the carboxyl group of key amino acids of CYP2C9 at Leu362, CYP2C19 at Ile362, and CYP2D6 at Val370 (Figures 4 and 5). These amino acids were also involved in their selective inhibitor-binding interactions (Table 1). However, both Ag_3 clusters did not interact directly with any amino acid residues within the inhibitor binding sites of CYP1A2, CYP2E1, and CYP3A4 (Figures 4 and 5, Table 1). According to these results, sharing of amino acid interactions with the selective inhibitors implied that AgNPs potentially inhibit CYP2C9, CYP2C19, and CYP2D6 enzyme activities.

Table 1. Interactions of Specific CYP Inhibitors, Ag^+, and Ag_3 Cluster with Amino Acid Residues within the Binding Site Pocket of CYP Enzymes

CYP isoform	PDB	ligand	amino acid residues
CYP1A2	2hi4	furafylline	Thr124, Ala317, Asp320
		Ag^+	Ser232, Thr385
		Ag_3 (D_{3h})	Pro383, Phe384, Leu497
		Ag_3 (C_{2v})	Phe384, Tyr495, Gly496, Leu497
CYP2C9	1r9o	sulfaphenazole	Thr301, Leu362
		Ag^+	Met426
		Ag_3 (D_{3h})	Leu362, Pro427
		Ag_3 (C_{2v})	Asp360, Leu361, Leu362, Pro427
CYP2C19	4gqs	*N*-3-benzyl phenobarbital	Ala297, Thr301, Ile362, Leu366
		Ag^+	Phe448, Phe451
		Ag_3 (D_{3h})	Gln356, Asp360, Ile362
		Ag_3 (C_{2v})	Gln356, Asp360, Ile362
CYP2D6	4xrz	quinidine	Ser304, Ala305, Val308, Val370, Phe483, Leu484
		Ag^+	Val227, Leu230, Leu231
		Ag_3 (D_{3h})	Ile369, Val370, Pro435
		Ag_3 (C_{2v})	Val370, Pro435
CYP2E1	3gph	4-methylpyrazole	Ala299
		Ag^+	His109, Arg112, Asp295
		Ag_3 (D_{3h})	Val364, Pro429
		Ag_3 (C_{2v})	Leu363, Val364
CYP3A4	5te8	ketoconazole	Ser119, Leu216, Phe304, Ala370, Arg372
		Ag^+	Phe367
		Ag_3 (D_{3h})	Pro368, Pro434
		Ag_3 (C_{2v})	Pro368, Ile369, Pro434

DOI: 10.1021/acs.jcim.9b00572
J. Chem. Inf. Model. 2019, 59, 5126−5134

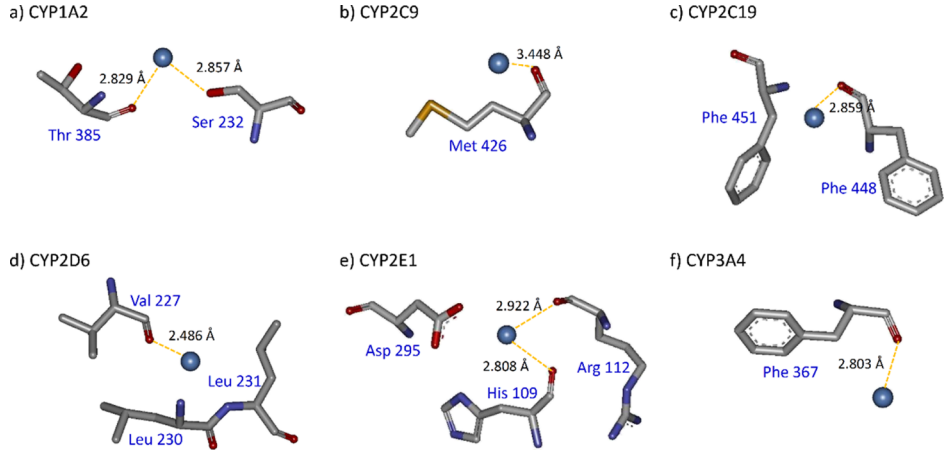

Figure 3. Molecular docking results of Ag^+ at the binding site of CYP enzymes: (a) CYP1A2, (b) CYP2C9, (c) CYP2C19, (d) CYP2D6, (e) CYP2E1, and (f) CYP3A4. All key amino acid residues are within a 3 Å radius of the Ag^+ ion.

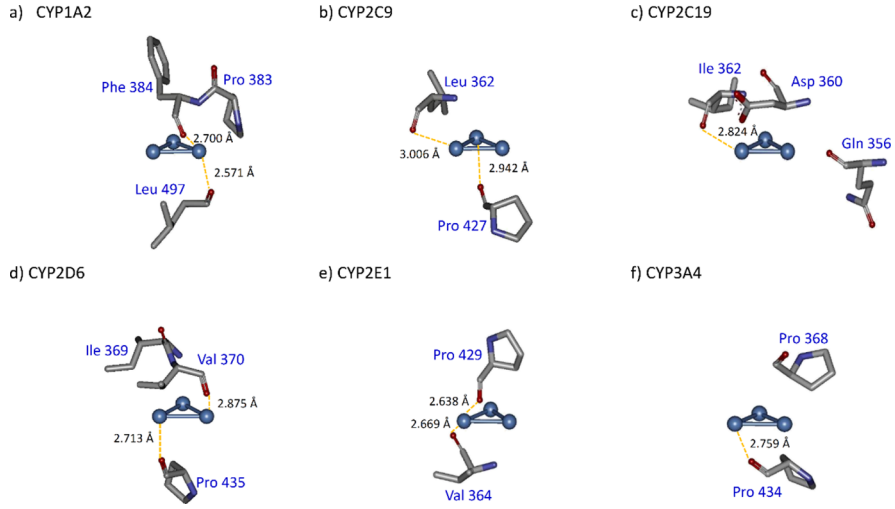

Figure 4. Docking results of the Ag_3 (D_{3h}) at the binding site of CYP enzymes: (a) CYP1A2, (b) CYP2C9, (c) CYP2C19, (d) CYP2D6, (e) CYP2E1, and (f) CYP3A4. All key amino acid residues are within a 3 Å radius of the Ag_3 cluster.

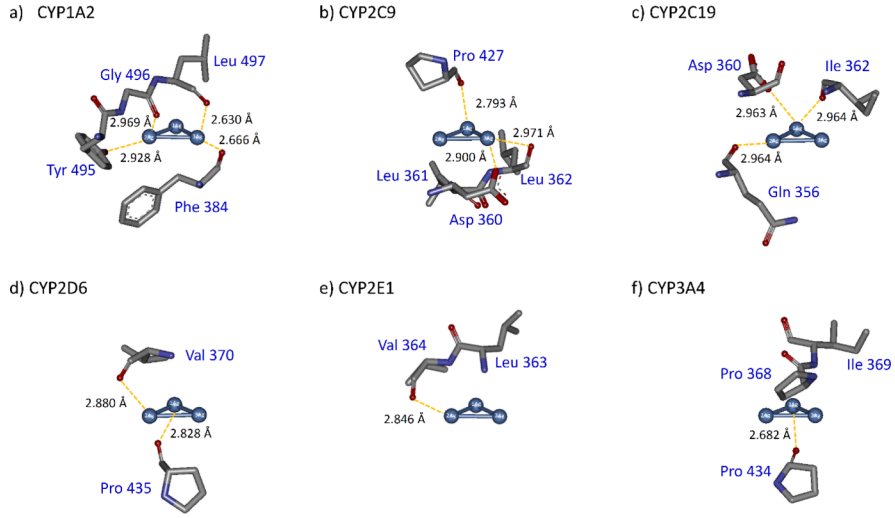

Figure 5. Docking results of the Ag_3 (C_{2v}) at the binding site of CYP enzymes: (a) CYP1A2, (b) CYP2C9, (c) CYP2C19, (d) CYP2D6, (e) CYP2E1, and (f) CYP3A4. All key amino acid residues are within a 3 Å radius of the Ag_3 cluster.

QM Calculations of CYP Enzymes−Ag_3 Cluster Complexes. To further investigate mechanisms of potential CYP inhibitions, QM calculations were performed. The starting geometry of CYP enzymes−Ag_3 cluster complexes

DOI: 10.1021/acs.jcim.9b00572
J. Chem. Inf. Model. 2019, 59, 5126−5134

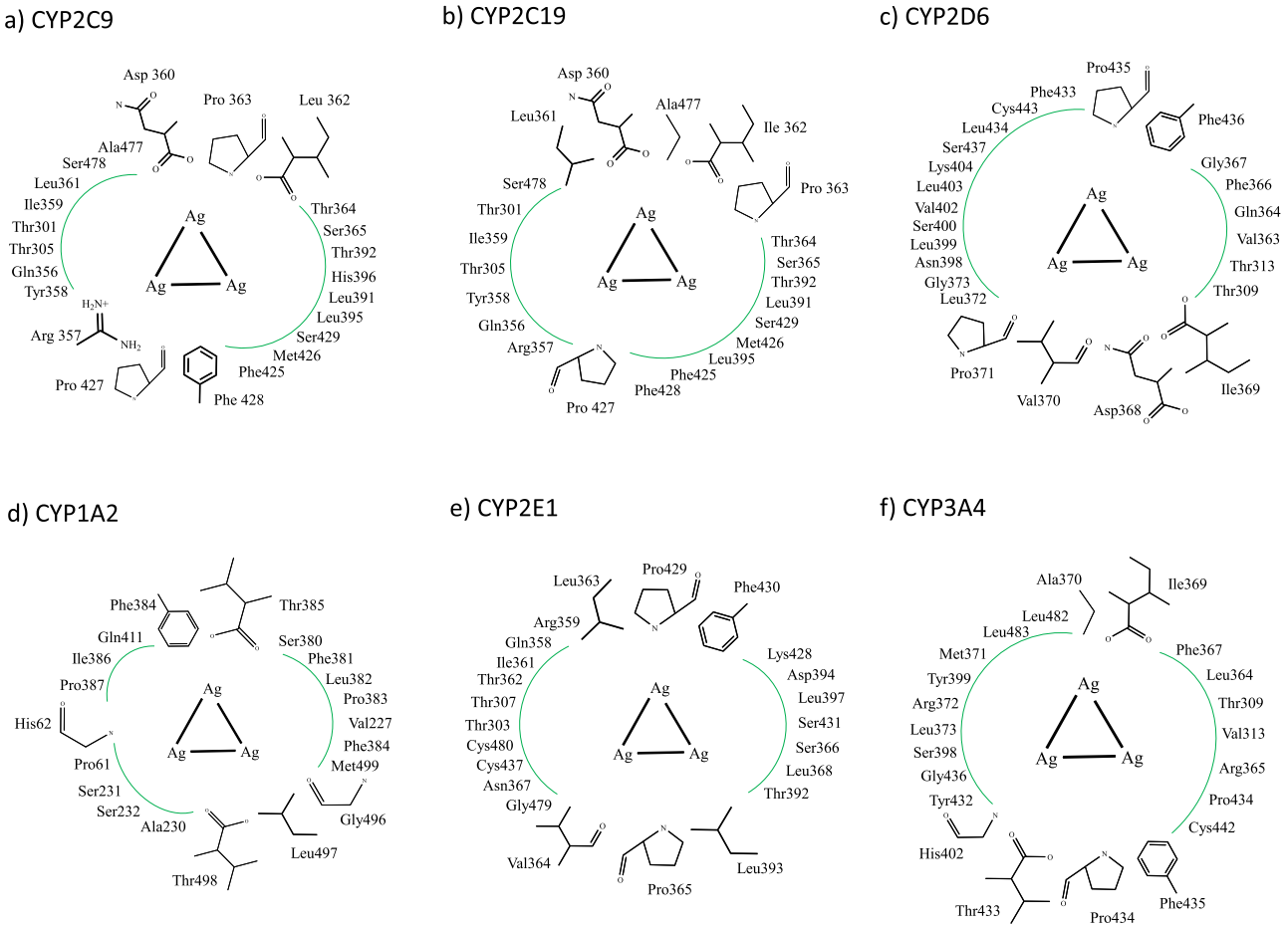

Figure 6. Schematic models of the Ag_3 cluster bound to (a) CYP2C9, (b) CYP2C19, (c) CYP2D6, (d) CYP1A2, (e) CYP2E1, and (f) CYP3A4 enzyme binding sites.

Table 2. Interaction Energies Including the ZPE Correction of the Ag_3 Cluster−Amino Acid Calculated by Using the M06-2X Method with 6-31g(d,p) Basis Set (in kcal/mol)

CYP1A2		CYP2C9		CYP2C19		CYP2D6		CYP2E1		CYP3A4	
amino acid residue	interaction energy (kcal/mol)	amino acid residue	interaction energy (kcal/mol)	amino acid residue	interaction energy (kcal/mol)	amino acid residue	interaction energy (kcal/mol)	amino acid residue	interaction energy (kcal/mol)	amino acid residue	interaction energy (kcal/mol)
His62	−4.15	Arg357	−9.29	Gln356	−12.68	Asp368	−28.32	Leu363	−18.38	Ile369	−18.52
Phe384	−22.46	Asp360	−42.19	Asp360	−39.58	Ile369	−19.62	Val364	−23.62	Ala370	−16.35
Thr385	−22.33	Leu362	−21.65	Leu361	−19.86	Val370	−22.99	Pro365	−19.67	His402	−6.62
Gly496	−14.05	Pro363	−14.85	Ile362	−107.63	Pro371	−15.60	Leu393	−10.46	Thr433	−8.29
Leu497	−27.71	Pro427	−19.54	Pro363	−20.76	Pro435	−17.81	Pro429	−18.51	Pro434	−14.19
Thr498	−18.42	Phe428	−16.43	Pro427	−15.76	Phe436	−15.71	Phe430	−16.14	Phe435	−14.89

for the QM study was obtained from the molecular docking simulation. The CYP enzymes−Ag_3 cluster complexes were optimized accordingly using the B3LYP method to describe the QM region. The QM calculations of all amino acids of an individual chain fragment were completed (capped) with the acetyl and *N*-methyl groups replacing the prior and the following residues, respectively. Then, hydrogen atoms were added to the obtained model system, which was performed by using the semi-empirical PM6 method, implemented by the Gaussian 09 program.[30] Therefore, hydrogen atoms of amino acid residues and all atoms of Ag_3 cluster were optimized. The results obtained from the QM calculations of the structure of CYP enzymes−Ag_3 cluster complexes showed that all amino acid residues were located with at least one atom interacting with an Ag atom in the Ag_3 clusters within the distances of 7 Å. Then, the amino acids were selected to calculate the interaction energy with the Ag_3 cluster based on QM calculations. The QM calculation results of CYP2C9 showed that 24 residues (Thr301, Thr305, Val355-Gln356-Arg357-Tyr358-Ile359-Asp360-Leu361-Leu362-Pro363-Thr364-Ser365, Leu391-Thr392, Leu395-His396, Phe425-Met426-Pro427-Phe428- Ser429, and Ala477-Ser478) were surrounded in the binding sites of CYP2C9 (Figure 6a). There were strong interactions between the Ag_3 cluster and Arg357, Asp360, Leu362, Pro363, Pro427, and Phe428, with the interaction energy of about −9.29, −42.19, −21.65, −14.85, −19.54, and −16.43 kcal/mol, respectively (Table 2). In addition, it was found that the Ag_3 cluster interacted with the oxygen atom of

DOI: 10.1021/acs.jcim.9b00572
J. Chem. Inf. Model. 2019, 59, 5126−5134

Table 3. Second-Order Perturbation Theory Analysis of Fock Matrix in NBO Basis for Ag_3 Cluster−Amino Acid Complexes Optimized by Using the M06-2X/6-31G(d,p) Method

CYP enzymes	complex	donor NBO (i)	acceptor NBO (j)	$E(2)$ (kcal/mol)	$E(j) - E(i)$ (a.u.)	$F_{(i,j)}$ (a.u.)
CYP2C9	Ag_3 cluster−Leu362	LP-O	LP*-Ag	3.87	0.84	0.072
	Ag_3 cluster−Pro427	LP-O	LP*-Ag	4.54	0.84	0.078
CYP2C19	Ag_3 cluster−Gln356	LP-O	LP*-Ag	4.32	0.88	0.078
	Ag_3 cluster−Asp360	LP-O	LP*-Ag	5.01	0.7	0.075
	Ag_3 cluster−Ile362	LP-N	LP*-Ag	3.63	0.45	0.052
CYP2D6	Ag_3 cluster−Ile369	LP-N	LP*-Ag	0.48	0.41	0.019
	Ag_3 cluster−Val370	LP-O	LP*-Ag	3.81	0.84	0.072
	Ag_3 cluster−Pro435	LP-O	LP*-Ag	4.12	0.84	0.075

carbonyl group of amino acid residues Arg357, Leu362, Pro363, Pro427, and Phe428 at a distance of 3.260, 2.971, 2.973, 2.703, and 2.705 Å, respectively (Figure S2 of the Supporting Information). Interestingly, QM calculations confirmed that Leu362 and Pro427 were the key amino acids of CYP2C9−Ag_3 cluster complex, which associated with the CYP2C9 inhibition.

The results obtained from CYP2C19−Ag_3 cluster interaction were similar to that of CYP2C9, with additional two amino acid residues, Ser393 and Val394 (Figure 6b). The QM calculation results demonstrated that the Ag_3 cluster strongly interacted with Gln356, Asp360, Leu361, Ile362, Pro363, and Pro427 amino acid residues of CYP2C19, with the energy of about −12.68, −39.58, −19.86, −107.63, −20.76, and −15.76 kcal/mol, respectively (Table 2). Among them, Asp360 had the strongest interaction. Furthermore, Ile362, Asp360, and Gln356 residues formed strong bonds with the Ag_3 cluster with corresponding distances of 2.231, 2.385, and 4.019 Å, respectively (Figure S3 of the Supporting Information). Indeed, QM calculations confirmed that Gln356, Asp360, and Ile362 were the key amino acids associated with of CYP2C19 inhibition by AgNPs.

For CYP2D6, QM calculations showed the binding of Ag_3 cluster with 31 amino acid residues, including Thr309-Thr310-Ser311-Thr312-Thr313, Val363-Gln364-Arg365-Phe366-Gly367-Asp368-Ile369-Val370-Pro371-Leu372-Gly373, Asn398-Leu399-Ser400-Ser401-Val402-Leu403-Lys404, Phe433-Leu434-Pro435-Phe436-Ser437, Cys443, and Leu484-Val485 (Figure 6c). The interaction energies of these amino acids are shown in Table 2. The Ag_3 cluster preferably bound to amino acids Asp368, Ile369, Val370, Pro371, Pro435, and Phe436, with interaction energies of about −28.32, −19.62, −22.99, −15.16, −17.81, and −15.71 kcal/mol, respectively. The measured distances between the Ag_3 cluster and Asp368, Ile369, Val370, Pro371, Pro435, and Phe436 were 2.403, 2.404, 2.615, 3.268, 2.979, and 2.979 Å, respectively, as shown in Figure S4 of the Supporting Information. According to these results, even though Asp368 predominantly interacted with the Ag_3 cluster, Val370 was the key amino acid involved in the CYP2D6 inhibition.

For other CYP enzymes, from the molecular docking results, the Ag_3 cluster showed no interaction with any key amino acids of CYP1A2, CYP2E1, and CYP3A4 enzymes. The QM calculation results demonstrated that the binding pocket of CYP1A2 enzyme−Ag_3 cluster complex composed of the following amino acid residues: Pro61-His62, Val227, Ala230-Ser231-Ser232, Ser380-Phe381-Leu382-Pro383-Phe384-Thr385-Ile386-Pro387, Gln411, and Tyr495-Gly496-Leu497-Thr498-Met499 within 7 Å (Figure 6d). Among these amino acids, it was found that carbonyl groups of Phe384, Thr385, Leu497, and Thr498 interacted with the Ag_3 cluster with a very low interaction energy of −22.46, −22.33, −27.71, and −18.42 kcal/mol, respectively (Table 2), with the distance of 2.660, 2.661, 2.630, and 2.904 Å, respectively (Figure S5 of the Supporting Information). None of them were the key amino acids for CYP1A2 inhibition.

QM analysis showed that the Ag_3 cluster interacted with the CYP2E1 enzyme through 29 amino acid residues including Thr303-Thr304-Ser305-Thr306-Thr307, Gln358-Arg359-Phe360-Ile361-Thr362-Leu363-Val364-Pro365-Ser366-Asn367-Leu368, Thr392-Leu393-Asp394-Ser395-Val396-Leu397, Lys428-Pro429-Phe430-Ser431, Cys437, and Gly479-Cys480 (Figure 6e). The interaction between the Ag_3 cluster and five amino acid residues, including Leu363, Val364, Pro365, Pro429, and Phe430, demonstrated strong interaction with energies of −18.38, −23.62, −19.67, −18.51, and −16.14 kcal/mol, respectively (Table 2), and corresponding distance of 2.622, 2.413, 3.037, 2.763, and 3.518 Å, respectively (Figure S6 of the Supporting Information). These five amino acids were not associated with CYP2E1 inhibition.

Finally, using QM calculations, the CYP3A4 enzyme−Ag_3 cluster complex interacted with Thr309, Val313, Leu364-Arg365-Leu366-Phe367-Pro368-Ile369-Ala370-Met371-Arg372-Leu373, Ser398-Tyr399-Ala400-Leu401-His402, Tyr432-Thr433-Pro434-Phe435-Gly436, Cys442, and Leu482-Leu483 (Figure 6f). The calculated results clearly indicated that Ile369, Ala370, His402, Pro434, and Phe435 had a predominant interaction energy of −18.52, −16.35, −6.62, −14.19, and −14.89 kcal/mol, respectively, (Table 2) and bond lengths of 2.319, 2.527, 4.767, 2.989, and 2.764 Å, respectively (Figure S7 of the Supporting Information). These amino acids were not present in CYP3A4 inhibition.

Among six CYP isoforms investigated in this study, the Ag_3 cluster strongly interacted with the key amino acid residues in binding pockets of CYP2C9, CYP2C19, and CYP2D6 enzymes at their active sites of CYP inhibition. These findings strongly support our in vitro data, in which incubation of AgNPs with rat liver microsomes inhibited activities of CYP2C and CYP2D to metabolize their specific substrates in a dose-dependent manner but not that of CYP1A, CYP2E1, and CYP3A.[57] However, in vivo studies demonstrated that multiple-dose oral ingestion of commercial colloidal nanosilver suspension for 14 days in healthy volunteers caused no significant changes in clinical and physical outcomes, as well as no significant inhibition or induction of CYP enzyme activities,[58,59] consistent with the study in rats.[57] Even though detectable levels of silver were found in human serum,[58,59] as well as in the rat liver,[57] it was suggested that it was in the ionic form and not as AgNPs.[57−59] Therefore, the lack of any effects on CYP activities in vivo can be partly explained by the presented

DOI: 10.1021/acs.jcim.9b00572
J. Chem. Inf. Model. 2019, 59, 5126−5134

docking results that Ag^+ did not interact with any key amino acids of those CYP inhibition-binding pockets.

NBO Analysis. NBO analysis was performed on the interactions between the Ag_3 cluster and key amino acids including Leu362, Ile362, and Val370 for CYP2C9, CYP2C19, and CYP2D6 enzymes, respectively. The results demonstrated an intramolecular charge transfer interaction of lone pair (LP) electrons of oxygen and nitrogen atoms to the antibonding (acceptor) orbital of Ag. The structures of Ag_3 cluster−Leu362 and Ag_3 cluster−Val370 complex showed electron transferring from LP of oxygen atom to the LP* of Ag, leading to stabilization energies of 3.87 and 3.81 kcal/mol, respectively (Table 3) and the O−Ag bond distance of 2.971 and 2.970 Å, respectively (Figures S2 and S4). For the Ag_3 cluster−Ile362 complex, the bond distance (N−Ag) is equal to 2.886 Å (Figure S3), and the charge is transferred from the LP of nitrogen atom to the LP* of Ag, leading to stabilization energies of 3.63 kcal/mol (Table 3). All information of Ag_3 cluster−amino acid complex charge transfers is summarized in Table S1 of the Supporting Information. The results from NBO calculation suggest that oxygen and nitrogen as two prominent atoms are involved in charge transfer interaction with the silver.

CONCLUSIONS

CYP is an important enzyme system for drug metabolism. Inhibition of CYP enzyme by coadministered drugs is clinically significant in terms of drug−drug interaction, which may reduce drug efficacy or increase toxicity. Therefore, inhibition of CYP enzymes by the Ag_3 cluster might link to potential AgNP−drug interaction. This study is to our knowledge, the first to use an in silico model to reveal molecular interactions between AgNPs and amino acids associated with CYP inhibition. Inhibition of particular CYP isoforms could be a potential "nanospecific effect" if a sufficient amount of AgNPs was exposed to the enzymes. In addition, it was suggested that the Ag_3 cluster was a minimal geometrical model for docking analysis. The amino acids Leu362, Ile362, and Val370 played key roles in AgNP-mediated inhibition of CYP2C9, CYP2C19, and CYP2D6, respectively. In the light of this finding, it is suggested that molecular docking together with QM analysis is a promising tool for predicting and understanding mechanisms of in vivo and in vitro CYP inhibition by NPs.

ASSOCIATED CONTENT

Supporting Information

The Supporting Information is available free of charge at https://pubs.acs.org/doi/10.1021/acs.jcim.9b00572.

Demonstration of NBO analysis, interactions between selective inhibitors and CYP enzymes by molecular docking, and QM calculations of Ag_3 cluster−amino acid complex of CYP enzymes (PDF)

AUTHOR INFORMATION

Corresponding Author

*E-mail: rawiwan.man@nstda.or.th. Phone: +66-2117-6850 ext. 6845. Fax: +66-2117-6851.

ORCID

Rawiwan Maniratanachote: 0000-0003-1475-1350

Notes

The authors declare no competing financial interest.

ACKNOWLEDGMENTS

This work was conducted while N.W. was a Postdoctoral Fellow at the National Science and Technology Development Agency (NSTDA). The authors acknowledge partial financial support from the Department of Chemistry, Faculty of Science, Srinakharinwirot University, Thailand. We thank Dr. Kevin Roy (Department of Genetics, Stanford University) and Prof. Dr. Supapan Seraphin (University of Arizona) for helpful comments and revising of the manuscript.

REFERENCES

(1) Vance, M. E.; Kuiken, T.; Vejerano, E. P.; McGinnis, S. P.; Hochella, M. F., Jr.; Rejeski, D.; Hull, M. S. Nanotechnology in the real world: Redeveloping the nanomaterial consumer products inventory. *Beilstein J. Nanotechnol.* **2015**, *6*, 1769−1780.

(2) Becaro, A. A.; Puti, F. C.; Correa, D. S.; Paris, E. C.; Marconcini, J. M.; Ferreira, M. D. Polyethylene films containing silver nanoparticles for applications in food packaging: Characterization of physico-chemical and anti-microbial properties. *J. Nanosci. Nanotechnol.* **2015**, *15*, 2148−2156.

(3) Boonkaew, B.; Kempf, M.; Kimble, R.; Supaphol, P.; Cuttle, L. Antimicrobial efficacy of a novel silver hydrogel dressing compared to two common silver burn wound dressings: Acticoat and PolyMem Silver®. *Burns* **2014**, *40*, 89−96.

(4) Edwards-Jones, V. The benefits of silver in hygiene, personal care and healthcare. *Lett. Appl. Microbiol.* **2009**, *49*, 147−152.

(5) Guzman, M.; Dille, J.; Godet, S. Synthesis and antibacterial activity of silver nanoparticles against gram-positive and gram-negative bacteria. *Nanomedicine* **2012**, *8*, 37−45.

(6) Rogers, K. R.; Navratilova, J.; Stefaniak, A.; Bowers, L.; Knepp, A. K.; Al-Abed, S. R.; Potter, P.; Gitipour, A.; Radwan, I.; Nelson, C.; Bradham, K. D. Characterization of engineered nanoparticles in commercially available spray disinfectant products advertised to contain colloidal silver. *Sci. Total Environ.* **2018**, *619−620*, 1375−1384.

(7) Kim, Y. S.; Kim, J. S.; Cho, H. S.; Rha, D. S.; Kim, J. M.; Park, J. D.; Choi, B. S.; Lim, R.; Chang, H. K.; Chung, Y. H.; Kwon, I. H.; Jeong, J.; Han, B. S.; Yu, I. J. Twenty-eight-day oral toxicity, genotoxicity, and gender-related tissue distribution of silver nanoparticles in Sprague Dawley rats. *Inhal. Toxicol.* **2008**, *20*, 575−583.

(8) Kim, Y. S.; Song, M. Y.; Park, J. D.; Song, K. S.; Ryu, H. R.; Chung, Y. H.; Chang, H. K.; Lee, J. H.; Oh, K. H.; Kelman, B. J.; Hwang, I. K.; Yu, I. J. Subchronic oral toxicity of silver nanoparticles. *Part. Fibre Toxicol.* **2010**, *7*, 20.

(9) Sung, J. H.; Ji, J. H.; Park, J. D.; Yoon, J. U.; Kim, D. S.; Jeon, K. S.; Song, M. Y.; Jeong, J.; Han, B. S.; Han, J. H.; Chung, Y. H.; Chang, H. K.; Lee, J. H.; Cho, M. H.; Kelman, B. J.; Yu, I. J. Subchronic inhalation toxicity of silver nanoparticles. *Toxicol. Sci.* **2009**, *108*, 452−461.

(10) Tang, J.; Xiong, L.; Wang, S.; Wang, J.; Liu, L.; Li, J.; Yuan, F.; Xi, T. Distribution, translocation and accumulation of silver nanoparticles in rats. *J. Nanosci. Nanotechnol.* **2009**, *9*, 4924−4932.

(11) Guengerich, F. P. Cytochrome P450 and chemical toxicology. *Chem. Res. Toxicol.* **2008**, *21*, 70−83.

(12) Lin, J. H.; Lu, A. Y. H. Inhibition and induction of cytochrome P450 and the clinical implications. *Clin. Pharmacokinet.* **1998**, *35*, 361−390.

(13) Pelkonen, O.; Turpeinen, M.; Hakkola, J.; Honkakoski, P.; Hukkanen, J.; Raunio, H. Inhibition and induction of human cytochrome P450 enzymes: current status. *Arch. Toxicol.* **2008**, *10*, 667−715.

(14) Martignoni, M.; Groothuis, G. M. M.; de Kanter, R. Species differences between mouse, rat, dog, monkey and human CYP-mediated drug metabolism, inhibition and induction. *Expert Opin. Drug Metab. Toxicol.* **2006**, *2*, 875−894.

(15) Sewell, F.; Aggarwal, M.; Bachler, G.; Broadmeadow, A.; Gellatly, N.; Moore, E.; Robinson, S.; Rooseboom, M.; Stevens, A.;

DOI: 10.1021/acs.jcim.9b00572
J. Chem. Inf. Model. 2019, 59, 5126−5134

Terry, C.; Burden, N. The current status of exposure driven approaches for chemical safety assessment: A cross-sector perspective. *Toxicology* **2017**, *389*, 109−117.
(16) Gowri, S.; Gopinath, K.; Arumugam, A. Experimental and computational assessment of mycosynthesized CdO nanoparticles towards biomedical applications. *J. Photochem. Photobiol. B.* **2018**, *180*, 166−174.
(17) Carreño-Fuentes, L.; Bahena, D.; Palomares, L.; Ramírez, O.; José-Yacamán, M.; Plascencia-Villa, G. Molecular docking and aberration-corrected STEM of palladium nanoparticles on viral templates. *Metals* **2016**, *6*, 200.
(18) Cohen, S.; Kozuch, S.; Hazan, C.; Shaik, S. Does substrate oxidation determine the regioselectivity of cyclohexene and propene oxidation by cytochrome P450? *J. Am. Chem. Soc.* **2006**, *128*, 11028−11029.
(19) Lonsdale, R.; Harvey, J. N.; Mulholland, A. J. Compound I reactivity defines alkene oxidation selectivity in cytochrome P450cam. *J. Phys. Chem. B* **2010**, *114*, 1156−1162.
(20) Bathelt, C. M.; Mulholland, A. J.; Harvey, J. N. QM/MM modeling of benzene hydroxylation in human cytochrome P450 2C9. *J. Phys. Chem. A* **2008**, *112*, 13149−13156.
(21) Schyman, P.; Lai, W.; Chen, H.; Wang, Y.; Shaik, S. The directive of the protein: how does cytochrome P450 select the mechanism of dopamine formation? *J. Am. Chem. Soc.* **2011**, *133*, 7977−7984.
(22) Lonsdale, R.; Houghton, K. T.; Żurek, J.; Bathelt, C. M.; Foloppe, N.; de Groot, M. J.; Harvey, J. N.; Mulholland, A. J. Quantum mechanics/molecular mechanics modeling of regioselectivity of drug metabolism in cytochrome P450 2C9. *J. Am. Chem. Soc.* **2013**, *135*, 8001−8015.
(23) Walsh, A. A.; Szklarz, G. D.; Scott, E. E. Human cytochrome P450 1A1 structure and utility in understanding drug and xenobiotic metabolism. *J. Biol. Chem.* **2013**, *288*, 12932−12943.
(24) Sansen, S.; Yano, J. K.; Reynald, R. L.; Schoch, G. A.; Griffin, K. J.; Stout, C. D.; Johnson, E. F. Adaptations for the oxidation of polycyclic aromatic hydrocarbons exhibited by the structure of human P450 1A2. *J. Biol. Chem.* **2007**, *282*, 14348−14355.
(25) Wester, M. R.; Yano, J. K.; Schoch, G. A.; Yang, C.; Griffin, K. J.; Stout, C. D.; Johnson, E. F. The structure of human cytochrome P450 2C9 complexed with flurbiprofen at 2.0-Å resolution. *J. Biol. Chem.* **2004**, *279*, 35630−35637.
(26) Hu, T.; Zhou, X.; Wang, L.; Or, P. M. Y.; Yeung, J. H. K.; Kwan, Y. W.; Cho, C. H. Effects of tanshinones from *salvia miltiorrhiza* on CYP2C19 activity in human liver microsomes: Enzyme kinetic and molecular docking studies. *Chem. Biol. Interact.* **2015**, *230*, 1−8.
(27) Brodney, M. A.; Beck, E. M.; Butler, C. R.; Barreiro, G.; Johnson, E. F.; Riddell, D.; Parris, K.; Nolan, C. E.; Fan, Y.; Atchison, K.; Gonzales, C.; Robshaw, A. E.; Doran, S. D.; Bundesmann, M. W.; Buzon, L.; Dutra, J.; Henegar, K.; LaChapelle, E.; Hou, X.; Rogers, B. N.; Pandit, J.; Lira, R.; Martinez-Alsina, L.; Mikochik, P.; Murray, J. C.; Ogilvie, K.; Price, L.; Sakya, S. M.; Yu, A.; Zhang, Y.; O'Neill, B. T. Utilizing structures of CYP2D6 and BACE1 complexes to reduce risk of drug-drug interactions with a novel series of centrally efficacious BACE1 inhibitors. *J. Med. Chem.* **2015**, *58*, 3223−3252.
(28) Porubsky, P. R.; Battaile, K. P.; Scott, E. E. Human cytochrome P450 2E1 structures with fatty acid analogs reveal a previously unobserved binding mode. *J. Biol. Chem.* **2010**, *285*, 22282−22290.
(29) Sevrioukova, I. F.; Poulos, T. L. Structural basis for regiospecific midazolam oxidation by human cytochrome P450 3A4. *Proc. Natl. Acad. Sci. U.S.A.* **2017**, *114*, 486−491.
(30) Frisch, M. J.; Trucks, G. W.; Schlegel, H. B.; Scuseria, G. E.; Robb, M. A.; Cheeseman, J. R.; Scalmani, G.; Barone, V.; Mennucci, B.; Petersson, G. A.; Nakatsuji, H.; Caricato, M.; Li, X.; Hratchian, H. P.; Izmaylov, A. F.; Bloino, J.; Zheng, G.; Sonnenberg, J. L.; Hada, M.; Ehara, M.; Toyota, K.; Fukuda, R.; Hasegawa, J.; Ishida, M.; Nakajima, T.; Honda, Y.; Kitao, O.; Nakai, H.; Vreven, T.; Montgomery, J. A., Jr.; Peralta, J. E.; Ogliaro, F.; Bearpark, M.; Heyd, J. J.; Brothers, E.; Kudin, K. N.; Staroverov, V. N.; Kobayashi, R.; Normand, J.; Raghavachari, K.; Rendell, A.; Burant, J. C.; Iyengar, S. S.; Tomasi, J.; Cossi, M.; Rega, N.; Millam, N. J.; Klene, M.; Knox, J. E.; Cross, J. B.; Bakken, V.; Adamo, C.; Jaramillo, J.; Gomperts, R.; Stratmann, R. E.; Yazyev, O.; Austin, A. J.; Cammi, R.; Pomelli, C.; Ochterski, J. W.; Martin, R. L.; Morokuma, K.; Zakrzewski, V. G.; Voth, G. A.; Salvador, P.; Dannenberg, J. J.; Dapprich, S.; Daniels, A. D.; Farkas, Ö.; Foresman, J. B.; Ortiz, J. V.; Cioslowski, J.; Fox, D. J. *Gaussian 09*, Revision E.01, 2009.
(31) Morris, G. M.; Huey, R.; Lindstrom, W.; Sanner, M. F.; Belew, R. K.; Goodsell, D. S.; Olson, A. J. AutoDock4 and AutoDockTools4: automated docking with selective receptor flexibility. *J. Comput. Chem.* **2009**, *30*, 2785−2791.
(32) Dassault Systemes BIOVIA. *Discovery Studio Modeling Environment, Release 2017*; Dassault Systemes: San Diego, 2017.
(33) Zhao, Y.; Truhlar, D. G. The M06 suite of density functionals for main group thermochemistry, thermochemical kinetics, noncovalent interactions, excited states, and transition elements: two new functionals and systematic testing of four M06-class functionals and 12 other functionals. *Theor. Chem. Acc.* **2008**, *120*, 215−241.
(34) Tamer, Ö.; Bhatti, M. H.; Yunus, U.; Nadeem, M.; Avcı, D.; Atalay, Y.; Yaqub, A.; Quershi, R. Structure-property relationship of 3-(N-phthalimidomethyl)-4-amino-1,2,4-triazole-5-thione: A structural, spectroscopic and DFT study. *J. Mol. Struct.* **2017**, *1133*, 329−337.
(35) Stewart, J. J. P. Optimization of parameters for semiempirical methods V: Modification of NDDO approximations and application to 70 elements. *J. Mol. Model.* **2007**, *13*, 1173−1213.
(36) Dahlke, E. E.; Olson, R. M.; Leverentz, H. R.; Truhlar, D. G. Assessment of the accuracy of density functionals for prediction of relative energies and geometries of low-lying isomers of water hexamers. *J. Phys. Chem. A* **2008**, *112*, 3976−3984.
(37) Larson, L. J.; Kuno, M.; Tao, F.-M. Hydrolysis of sulfur trioxide to form sulfuric acid in small water clusters. *J. Chem. Phys.* **2000**, *112*, 8830−8838.
(38) Gangadharan, R. P.; Sampath Krishnan, S. Natural bond orbital (NBO) population analysis of 1-Azanapthalene-8-ol. *Acta Phys. Pol., A* **2014**, *125*, 18−22.
(39) Samanta, B.; Sengupta, T.; Pal, S. Specificity of amino acid−aluminum cluster interaction and subsequent oxygen activation by the above complex. *J. Phys. Chem. C* **2018**, *122*, 28310−28323.
(40) Buglak, A. A.; Ramazanov, R. R.; Kononov, A. I. Silver cluster−amino acid interactions: a quantum-chemical study. *Amino Acids* **2019**, *51*, 855−864.
(41) Fournier, R. Theoretical study of the structure of silver clusters. *J. Chem. Phys.* **2001**, *115*, 2165−2177.
(42) McKee, M. L.; Samokhvalov, A. Density functional study of neutral and charged silver clusters Ag_n with n = 2-22. Evolution of properties and structure. *J. Phys. Chem. A* **2017**, *121*, 5018−5028.
(43) Li, Y.-F.; Li, Y.; Li, Y.; Tan, J.-J.; Li, H.-L. Structural and electronic properties of small silver-sulfur clusters: A density functional study. *Phys. B* **2016**, *499*, 29−37.
(44) Zhao, J.; Luo, Y.; Wang, G. Tight-binding study of structural and electronic properties of silver clusters. *Eur. Phys. J. D* **2001**, *14*, 309−316.
(45) Wang, Y.; Gong, X. G. First-principles study of neutral and charged silver clusters. *Eur. Phys. J. D* **2005**, *34*, 19−22.
(46) Huda, M. N.; Ray, A. K. Electronic structures and magic numbers of small silver clusters: a many-body perturbation-theoretic study. *Phys. Rev. A: At., Mol., Opt. Phys.* **2003**, *67*, 013201.
(47) Shao, X.; Liu, X.; Cai, W. Structural optimization of silver clusters up to 80 atoms with gupta and sutton-chen potentials. *J. Chem. Theory Comput.* **2005**, *1*, 762−768.
(48) Chen, M.; Dyer, J. E.; Li, K.; Dixon, D. A. Prediction of structures and atomization energies of small silver clusters, $(Ag)_n$, n < 100. *J. Phys. Chem. A* **2013**, *117*, 8298−8313.
(49) Yang, X.; Cai, W.; Shao, X. Structural variation of silver clusters from Ag_{13} to Ag_{160}. *J. Phys. Chem. A* **2007**, *111*, 5048−5056.
(50) Kunze, K. L.; Trager, W. F. Isoform-selective mechanism-based inhibition of human cytochrome P450 1A2 by furafylline. *Chem. Res. Toxicol.* **1993**, *6*, 649−656.

DOI: 10.1021/acs.jcim.9b00572
J. Chem. Inf. Model. 2019, 59, 5126−5134

(51) Back, D.; Tjia, J.; Karbwang, J.; Colbert, J. *In vitro* inhibition studies of tolbutamide hydroxylase activity of human liver microsomes by azoles, sulphonamides and quinolines. *Br. J. Clin. Pharmacol.* **1988**, *26*, 23−29.
(52) Baldwin, S. J.; Bloomer, J. C.; Smith, G. J.; Ayrton, A. D.; Clarke, S. E.; Chenery, R. J. Ketoconazole and sulphaphenazole as the respective selective inhibitors of P4503A and 2C9. *Xenobiotica* **1995**, *25*, 261−270.
(53) Suzuki, H.; Kneller, M. B.; Haining, R. L.; Trager, W. F.; Rettie, A. E. (+)-N-3-Benzylnirvanol and (-)-N-3-benzyl-phenobarbital: new potent and selective in vitro inhibitors of CYP2C19. *Drug Metab. Dispos.* **2002**, *30*, 235−239.
(54) Cai, X.; Wang, R. W.; Edom, R. W.; Evans, D. C.; Shou, M.; Rodrigues, A. D.; Liu, W.; Dean, D. C.; Baillie, T. A. Validation of (-)-N-3-benzyl-phenobarbital as a selective inhibitor of CYP2C19 in human liver microsomes. *Drug Metab. Dispos.* **2004**, *32*, 584−586.
(55) Broly, F.; Libersa, C.; Lhermitte, M.; Bechtel, P.; Dupuis, B. Effect of quinidine on the dextromethorphan O-demethylase activity of microsomal fractions from human liver. *Br. J. Clin. Pharmacol.* **1989**, *28*, 29−36.
(56) Collom, S. L.; Laddusaw, R. M.; Burch, A. M.; Kuzmic, P.; Perry, M. D., Jr.; Miller, G. P. CYP2E1 Substrate Inhibition. *J. Biol. Chem.* **2008**, *283*, 3487−3496.
(57) Kulthong, K.; Maniratanachote, R.; Kobayashi, Y.; Fukami, T.; Yokoi, T. Effects of silver nanoparticles on rat hepatic cytochrome P450 enzyme activity. *Xenobiotica* **2012**, *42*, 854−862.
(58) Munger, M. A.; Hadlock, G.; Stoddard, G.; Slawson, M. H.; Wilkins, D. G.; Cox, N.; Rollins, D. Assessing orally bioavailable commercial silver nanoparticle product on human cytochrome P450 enzyme activity. *Nanotoxicology* **2015**, *9*, 474−481.
(59) Munger, M. A.; Radwanski, P.; Hadlock, G. C.; Stoddard, G.; Shaaban, A.; Falconer, J.; Grainger, D. W.; Deering-Rice, C. E. *In vivo* human time-exposure study of orally dosed commercial silver nanoparticles. *Nanomedicine* **2014**, *10*, 1−9.

DOI: 10.1021/acs.jcim.9b00572
J. Chem. Inf. Model. 2019, 59, 5126−5134